

Article

# Vertical Monotonic and Cyclic Responses of a Bucket in Over-Consolidated Clay

Jun Jiang <sup>1</sup>, Dong Wang <sup>1,2,\*</sup> and Dengfeng Fu <sup>1</sup>

<sup>1</sup> MOE Key Laboratory of Marine Environment and Ecology, Ocean University of China, 238 Songling Road, Qingdao 266100, China; junjiang@stu.ouc.edu.cn (J.J.); dengfeng.fu@ouc.edu.cn (D.F.)

<sup>2</sup> Laboratory for Marine Geology, National Laboratory for Marine Science and Technology, Qingdao 266061, China

\* Correspondence: dongwang@ouc.edu.cn; Tel.: +86-13165325292

**Abstract:** Bucket foundations, especially multi-bucket foundations, have become an alternative for large offshore wind turbines. Vertical responses of a single bucket are critical for the serviceability design of tripod or tetrapod bucket foundations. Centrifuge tests are conducted to investigate the responses of a single bucket under monotonic and symmetric cyclic loading in over-consolidated clay. The strength of clay is obtained by cone penetration tests. The monotonic vertical capacity measured in the centrifuge tests are compared with the finite element results, with errors less than 6%. The effects of the ratio of cyclic loading amplitude to vertical capacity (ranging between 0.37 and 0.64) and the number of cycles on the accumulation of vertical displacement and evolution of stiffness are explored. Simplified functions are proposed to predict the evolutions of dimensional and dimensionless stiffness.

**Keywords:** vertical capacity; cyclic loading; bucket foundations; clay; offshore wind turbine; centrifuge testing



**Citation:** Jiang, J.; Wang, D.; Fu, D. Vertical Monotonic and Cyclic Responses of a Bucket in Over-Consolidated Clay. *J. Mar. Sci. Eng.* **2023**, *11*, 2044. <https://doi.org/10.3390/jmse11112044>

Academic Editor: M. Dolores Esteban

Received: 26 September 2023

Revised: 22 October 2023

Accepted: 23 October 2023

Published: 25 October 2023



**Copyright:** © 2023 by the authors. Licensee MDPI, Basel, Switzerland. This article is an open access article distributed under the terms and conditions of the Creative Commons Attribution (CC BY) license (<https://creativecommons.org/licenses/by/4.0/>).

## 1. Introduction

With the expansion of offshore wind energy, bucket foundations have been developed and considered as an economic option to support wind turbines [1,2]. Compared to conventional piles or large diameter mono-piles, the bucket foundations are with smaller aspect ratios and can be installed conveniently into the seabed by jacking and assisted suction [3,4]. The bucket foundations used in the practical applications can be categorized as the mono-bucket and multi-bucket. The latter is usually composed of three or four buckets, designed to resist large overturning moments caused by the horizontal loading applied on the wind turbine and supporting structure [5,6]. The interactions between single buckets may be neglected given that the bucket spaces are sufficiently large [7,8], then the overturning moment is resisted by the compression of buckets downwind and tension of buckets upwind, as Figure 1 shows [9,10]. The responses of a single bucket under monotonic and cyclic vertical forces are critical for the design of multi-bucket foundations [11,12]. The geotechnical conditions at several sites of offshore wind farms (e.g., Houhu in China and Dogger Bank in England) are mainly clay over sand layers, while the clay layers are dominant over the depth between the mudline and the bucket tip [13,14]. The concern of this paper is the single bucket of the multi-bucket foundation in clay.

For the bucket foundations in clay, the monotonic compressive and tensile capacities have been studied through finite element (FE) simulations [15,16] and model tests [11,17,18]. The monotonic vertical capacity factors depended on the aspect ratio of the bucket, the soil non-homogeneity, and the bucket–soil adhesion factor [16,19]. Unlike the end-bearing mechanism for the compressive capacity as Figure 2a shows, the soil failure mechanism caused by the tension load became complicated due to suction developed at the base of the bucket foundation. As Figure 2b–d show, the mechanisms observed in the tensile

loading tests included the reverse end-bearing, pull-out of bucket, and pull-out of bucket and soil plug inside [3]. The tensile capacities were usually assumed to be lower than the compressive ones, for example, by 20% for sealed buckets and by even up to 30% for the unsealed [18].

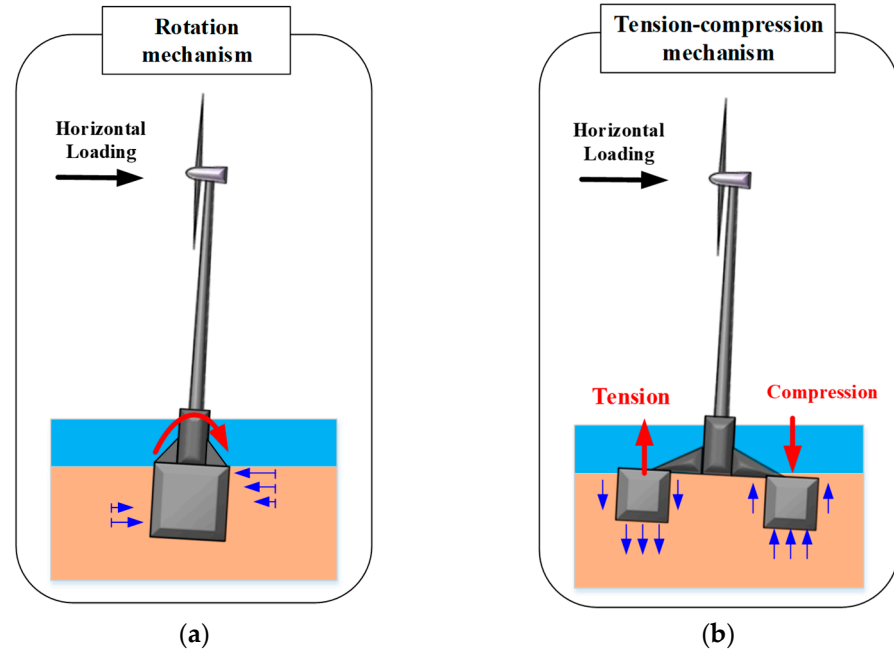


**Figure 1.** Response of bucket foundation subjected to horizontal loading: (a) Mono-bucket foundation; (b) Multi-bucket foundation.

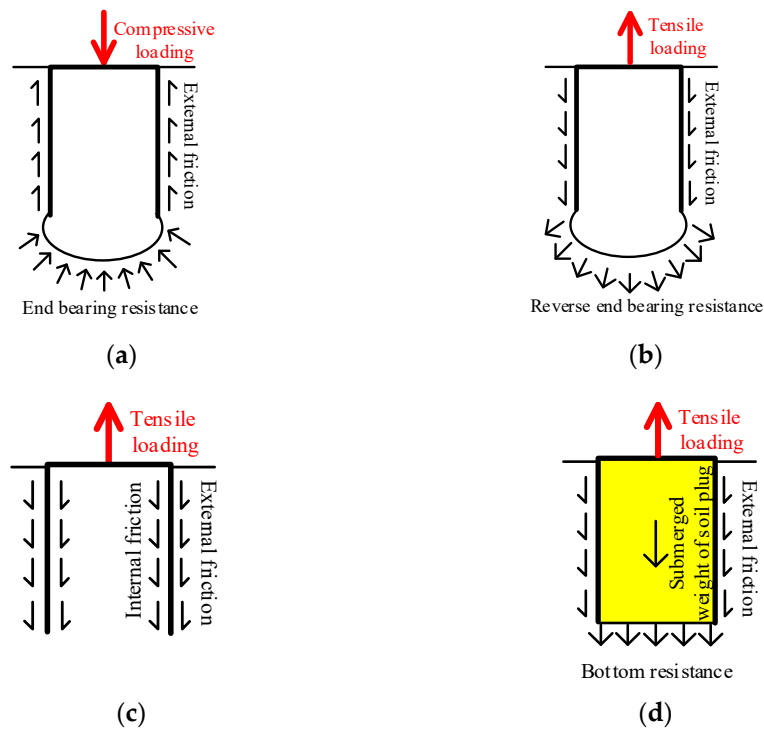


**Figure 2.** Resistances under compressive and tensile loadings: (a) End-bearing mechanism; (b) Reverse end-bearing mechanism; (c) Siding mechanism; (d) Pulling-out mechanism.

The magnitude and direction of vertical cyclic loading affected the displacement and stiffness of the bucket, and were quantified by  $\zeta_b$ , the ratio of the maximum loading

$V_{max}$  to the monotonic vertical capacity  $V_0$ , and  $\zeta_c$ , and the ratio of the minimum loading  $V_{min}$  to  $V_{max}$ , as Figure 3 shows [20]. Figure 3 also demonstrates the definitions of the loading amplitude  $V_c$  and average loading  $V_a$ . The displacements caused were defined, respectively, as the maximum  $w_{max}$ , the minimum  $w_{min}$ , and the average  $w_a$ , and the displacement amplitude was  $w_c$ . The studies on the vertical cyclic response of the bucket in clay were relatively limited, compared to those in sand and sand over clay [6,21–25]. For the bucket in sand, purely compressive loading ( $\zeta_c \geq 0$ ) and cycles with sufficiently large  $V_a$  on the compressive side led to downwards residual displacement which was approximately equal to  $w_a$  [24,26,27]. The load–displacement response became stiffer with  $N$  due to the soil hardening for one-way compressive loading, and the enhancement of stiffness is more obvious at higher  $V_a$  [6]. In contrast, upwards  $w_a$  occurred under zero and tensile average loading, independent of the  $V_c$  value [24]. The decrease in stiffness with  $N$  was more severe under zero average loading ( $\zeta_c = -1$ ) than that under one-way tensile loading [6,28], indicating loading with  $\zeta_c = -1$  may be more dangerous. For the bucket in sand over clay, the direction of  $w_a$  was also governed by  $V_a$  [25]. As for the bucket in clay, a few conventional [11,29] and centrifuge [30,31] model tests have been conducted. Given that the bucket was displaced under undrained conditions, the direction of  $w_a$  and the failure mechanism were a function of the direction of  $V_a$ : zero and tensile  $V_a$  led to upwards  $w_a$ , while compressive  $V_a$  larger than a small level, for example, 9% of the monotonic vertical capacity, may always generate downward  $w_a$  [31]. These phenomena of displacements were related to the positive excess pore pressure under compressive average loading and negative excess pore pressure under zero average loading [11]. At higher loading magnitudes, the accumulation of displacement was larger due to the more severe disturbance on soil. However, for loading magnitudes below a certain threshold, the bucket may be at a stable state without obvious residual displacement [31,32]. The displacement accumulated was observed under force-controlled loading, while the vertical resistance was degraded by about 35% in the first ~10 cycles and became stable at ~20 cycles if one-way cyclic loading with a small amplitude of ~0.009D was applied [33]. The stiffness was lower at higher  $V_c$  under purely compressive loading with  $\zeta_c = 0$  and a logarithmic function was used to describe the relationship between stiffness and the number of cycles [29]. For the bucket in clay subjected to cyclic loading, most existing studies were focused on the responses under horizontal cyclic loading [34–37]. The bucket under cyclic vertical loading was concerned in a limited number of recent studies only, such as by [29,33], however, their model tests were conducted at 1 g. Since the stress levels of soil are much lower than those in practical applications, the centrifuge test is preferred to provide more reliable data, especially for the loading with larger  $V_c$ .

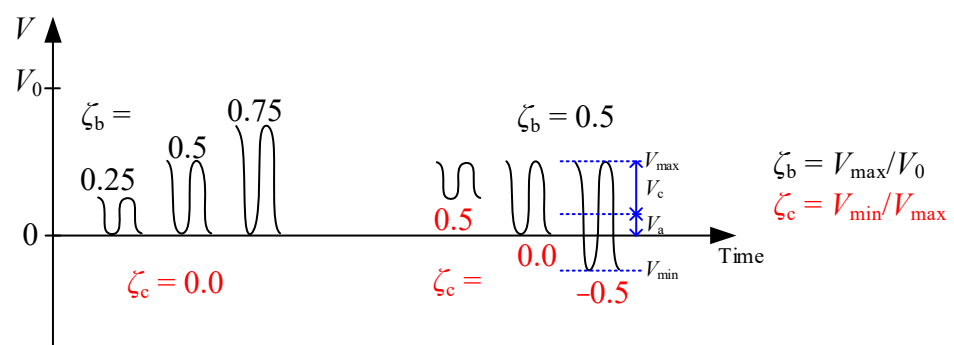


Figure 3. Definitions of  $V_{max}$ ,  $V_{min}$ ,  $\zeta_b$ ,  $\zeta_c$ ,  $V_c$ , and  $V_a$ .

In this paper, the load–displacement responses of the single bucket in clay under monotonic and symmetric cyclic vertical loading ( $\zeta_c = -1$ ) are investigated by centrifuge tests. The vertical capacities under monotonic loading are measured, validated by comparison with the finite element analyses. Then the accumulation of vertical displacement and the evolution of stiffness of the bucket are explored against various loading ampli-

tudes. As a result, simplified functions are proposed to predict the stiffness of the bucket under different loading amplitudes and number of cycles. Figure 4 shows the process of the methodology.

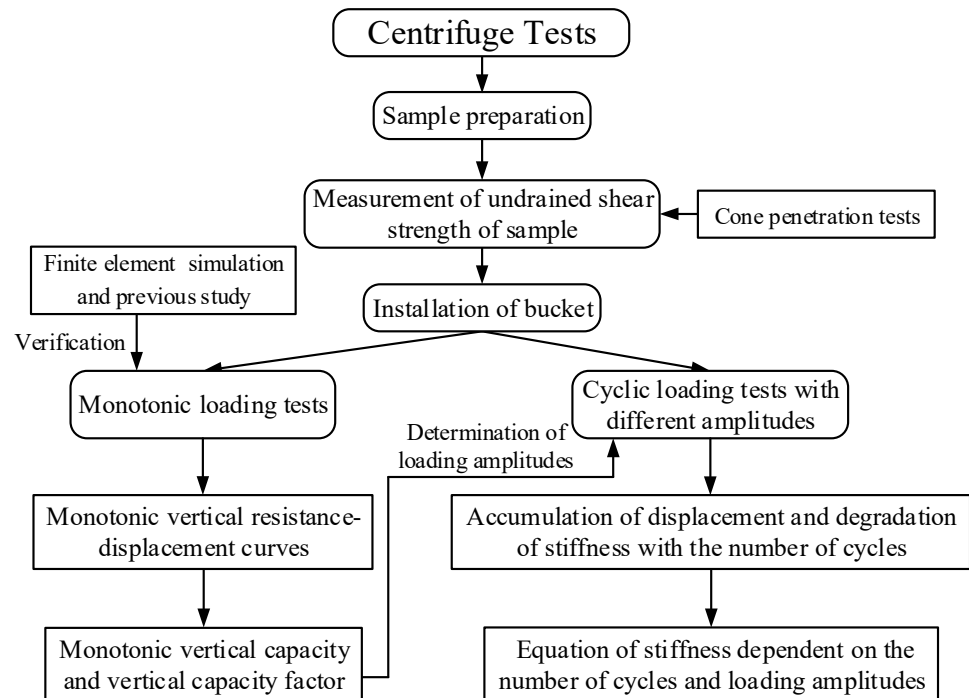


Figure 4. Process of the methodology.

## 2. Experimental Equipment and Soil Preparation

### 2.1. Experimental Equipment and Model Bucket

The tests were performed in a drum centrifuge with 1.4 m diameter at the Dalian University of Technology, China. Monotonic or cyclic vertical loads were applied on a bucket in over-consolidated kaolin clay. As Figure 5a,b show, the model bucket was made of aluminum alloy, with a diameter  $D$  of 40 mm, skirt length  $L$  of 40 mm, and skirt thickness  $t_s$  of 1 mm. Then the sizes in prototype were  $D = 4$  m,  $L = 4$  m, and  $t_s = 0.1$  m at an acceleration of 100 g. The skirt thickness ratio  $t_s/D$  of the model bucket was 0.025 which was larger than 0.005–0.008 in practice [38] to avoid buckling during installation in centrifuge. A vent was set on the bucket cap with a thickness of 3 mm. A load cell with a measurement range of 300 N and a laser displacement sensor with a precision of 0.01 mm, were used to measure the load and the vertical displacement of the bucket, as Figure 5c shows.

### 2.2. Sample Preparation and Strength Profile

To prepare the soil sample, dry clay powder was mixed with water in a vacuum tank for at least 4 h to form a slurry at a moisture content of twice the liquid limit. Table 1 demonstrates the properties of the clay. The slurry was then poured into a strongbox of 310 mm × 290 mm × 230 mm, followed by one-dimensional compression under 1 g conditions. The final pressure  $\sigma_v'$  was 90 kPa for Samples 1–3 and 60 kPa for Sample 4, with the compressions lasting about 38 and 36 d, respectively. The sensitivities,  $S_t$ , of clay samples in each strongbox were measured by vane shear tests with a range of 2.0–2.3 and an average value of 2.1. After consolidation, the samples were maintained wet throughout the tests by spraying water on the sample surfaces.

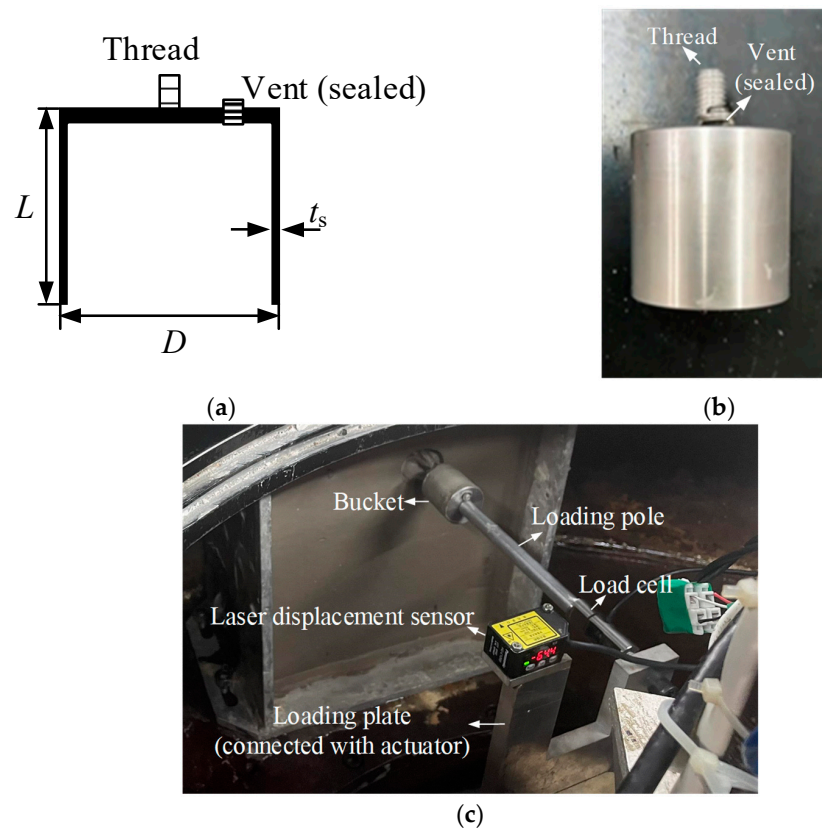


**Figure 5.** Model bucket and experimental apparatus: (a) Schematic model bucket; (b) Image of model bucket; (c) Experimental apparatus.

**Table 1.** Properties of kaolin clay.

Parameters	Values
Specific gravity, $G_s$	2.70
Effective unit weight, $\gamma'$ ( $\text{kN}/\text{m}^3$ )	6.97
Liquid limit (%)	42.8
Plastic limit (%)	20.8
Sensitivity, $S_t$	2.1
Vertical coefficient of consolidation, $c_v$ ( $\text{mm}^2/\text{s}$ ) ( $\sigma_v' = 60$ kPa)	0.11
Vertical coefficient of consolidation, $c_v$ ( $\text{mm}^2/\text{s}$ ) ( $\sigma_v' = 90$ kPa)	0.14

To characterize the strength profile of clay, cone penetrometer tests (CPTs) were conducted prior to installation of the strongbox into the centrifuge, using a probe with a diameter  $d$  of 10 mm. The distances between the cone penetrometer and the strongbox boundaries or the circumferences of buckets were at least  $6d$ , to avoid the boundary effect. The penetration velocity  $v$  of cone was 4 mm/s, leading to dimensionless velocity  $V = vd/c_v = 363.6$  or 285.7 for  $\sigma_v' = 60$  or 90 kPa, respectively, where  $c_v$  is the vertical coefficient of consolidation. Refs. [39–41] suggested that undrained responses occurred at  $V > 30$ . With the cone resistance profiles measured during the CPTs, the undrained shear strength  $s_u$  was calculated as:

$$s_u = (q_t - \sigma_{v0})/N_{kt}, \tag{1}$$

where  $q_t$  is the cone resistance;  $\sigma_{v0}$  the total overburden pressure; and  $N_{kt}$  the cone factor, which ranged between 9 and 18 for typical clays [42–44].  $N_{kt}$  was taken as 15 in this study. Figure 6 demonstrates the strength profiles recorded during the CPTs at 1 g condition (solid lines) and the corresponding fitting curves (dash lines). The strength of the soil sample was typically increased with soil depth [45,46] and can be described as  $s_u = s_{um} + kz$ , where  $s_{um}$

is the undrained shear strength at clay surface and  $k$  is the gradient of strength with soil depth  $z$ . The soil depth  $z$  at 1 g condition was multiplied by 100 (as centrifuge tests at an acceleration of 100 g) to obtain strength profiles in the prototype scale. As a result,  $s_u$  (in the unit of kPa) in centrifuge was determined as  $6.5 + 0.55z$ ,  $11.6, 9.0 + 0.4z$ , and  $6.0 + 0.18z$  for Samples 1–4, where  $z$  was in the unit of m.

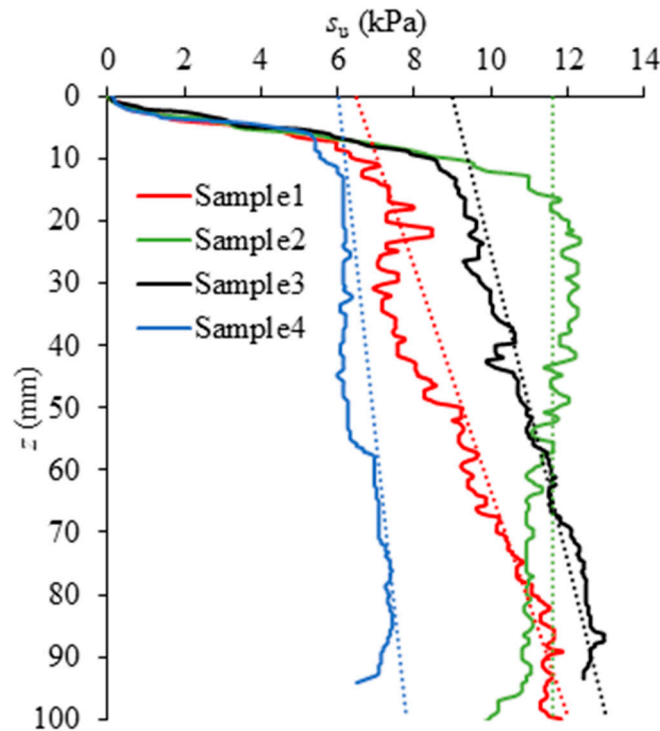


**Figure 6.** Strength profiles of the clay samples (the fitting curves of the strength profiles are shown as the dotted lines,  $N_{kt} = 15$ , model scale).

### 3. Experimental Arrangements

The model bucket was subjected to monotonic or cyclic loading after installation. For each strongbox, three locations were designed with one monotonic test and two cyclic tests. The distances between the bucket skirts and the strongbox sides were at least  $1.75D$ , while the distance from one skirt of a bucket to another was at least  $1.95D$ .

After the centrifuge was spun up to an acceleration level of 100 g, the bucket was jacked into soil at a velocity  $v$  of 1 mm/s. As the soil sample was consolidated at 60 or 90 kPa, the corresponding normalized velocity was  $V = vD/c_v = 363.6$  or  $285.7$ . The undrained response during installation was guaranteed since  $V$  was larger than 30. The vent on the cap of the bucket was open during installation, allowing the air/water inside the bucket to be expelled. When the bucket cap reached the soil surface, the penetration resistance increased quickly, indicating that the installation was completed. Then the centrifuge was stopped and the vent was sealed manually. This was to maintain the potential suction developed inside as the bucket was subjected to cyclic loading, which was similar to the operation in most practical applications. The centrifuge was spun up again to 100 g for the subsequent loading process.

In the monotonic loading tests, the bucket was penetrated at  $v = 1$  mm/s until the displacement reached a relatively large value of 10 mm ( $0.25L$ ), where the corresponding penetration resistance was defined as the monotonic capacity  $V_0$ .

In the cyclic loading tests, the loading amplitude  $V_c$  of the sinusoidal cyclic load was selected as a specified percentage of  $V_0$ , as Table 2 shows. Tests 2-3 and 4-3 were not presented here due to the unqualified precision of loading control. Only 6 cyclic loading tests were reported, with the ratios of loading amplitude to monotonic capacity,  $V_c/V_0$ ,

ranging between 0.37 and 0.64. It was expected to apply symmetric two-way cyclic loading since this was the most dangerous type of cyclic loading [3,47]. However, the average loading ratio,  $V_a/V_0$ , obtained were in the range of 0.01–0.05 due to limitations of the controlling system. The frequencies were controlled in the range of 0.5–0.84 Hz. When the frequency was 0.5 Hz, the corresponding dimensionless time factor  $T = c_v t/D^2$  over one cycle was  $1.4 \times 10^{-4}$  and  $1.8 \times 10^{-4}$  at  $c_v = 0.11$  and  $0.14 \text{ mm}^2/\text{s}$ , respectively.  $T$  became reduced with the frequency larger than 0.5 Hz. The response of clay over one cycle might be undrained given that  $T < 1.3 \times 10^{-3}$ , suggested by [48]. However, partial drainage may occur over dozens or hundreds of cycles, since  $T = 1.0$  was suggested to be associated with at least 90% consolidation [49,50]. Partial drainage was accompanied by an increase in the shear strength of soil. The cyclic tests were shut down after at least 650 cycles, or, when the maximum vertical displacement reached  $0.25L$ . Note that the compressive vertical loads and downward vertical displacements were taken positive in the following discussions.

**Table 2.** Experimental arrangements involving monotonic and cyclic tests.

Test No.	Load Type	$V_0$ (N)	$V_a/V_0$	$V_c/V_0$
1-1	Monotonic	129.3		
1-2	Cyclic		0.02	0.42
1-3	Cyclic		0.03	0.53
2-1	Monotonic	168.0		
2-2	Cyclic		0.01	0.58
3-1	Monotonic	160.6		
3-2	Cyclic		0.01	0.37
3-3	Cyclic		0.01	0.51
4-1	Monotonic	107.8		
4-2	Cyclic		0.05	0.64

#### 4. Installation

During installation, the penetration resistance is increased slowly prior to displacement of ~35 mm and then is enhanced rapidly, as Figure 7 shows. The abrupt change in the penetration resistance indicates the touchdown of the bucket cap. At the touchdown moments (solid points in Figure 7), the penetration resistance is changed from the sum of the friction resistances along both sides of the bucket skirt and the tip resistance to the sum of the friction resistance along the outside of the bucket and the end resistance. If the penetration resistance  $Q_{tot}$  at the touchdown moment is calculated as the sum of the friction resistance along both sides of the bucket skirt and the tip-bearing resistance, then  $Q_{tot} = z\alpha s_{ua}\pi(D + D_i) + (\gamma'z + s_{utip}N_c)A_{tip}$  [51], where  $\alpha$  is the adhesion factor;  $D_i$  is the internal diameter of bucket; and  $s_{ua}$  and  $s_{utip}$  are the average undrained shear strength along the bucket skirt and the undrained shear strength at the bucket tip, respectively;  $N_c$  is the bearing factor, usually taken as 7.5;  $A_{tip}$  is the cross-sectional area of the bucket tip. Figure 7a–d show  $Q_{tot}$  as 39.0, 58.1, 47.3, and 33.0 N, respectively, agreeing well with the results by [51] of 32.0, 50.4, 41.6, and 27.3 N with errors less than 18%. The depths of the touchdown points are slightly less than 37 mm (the bucket length minus the thickness of bucket cap), which is due to the soil plug formed during installation. The penetration resistance curves measured in each strongbox are close to each other, indicating that the prepared soil samples were uniform.

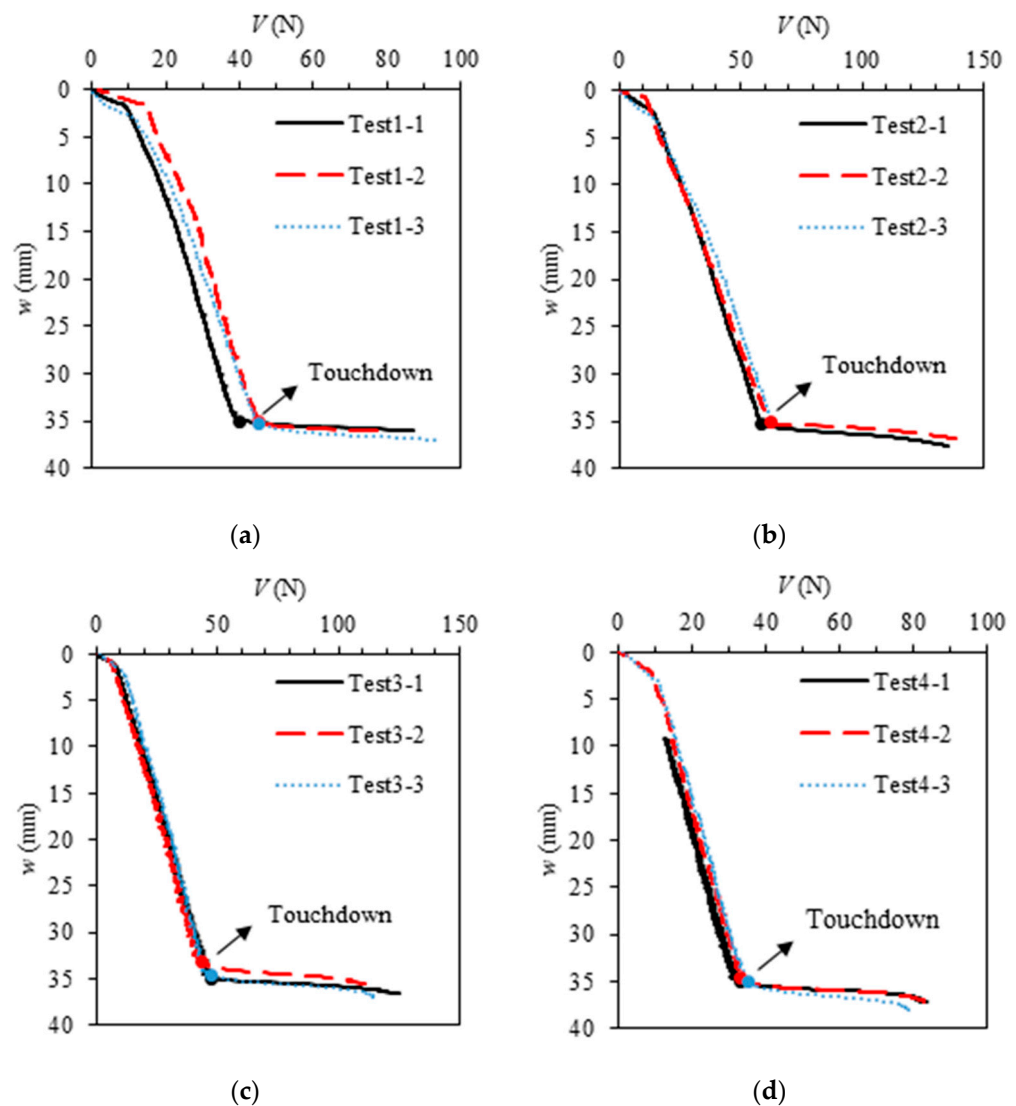


**Figure 7.** Penetration resistance–depth curves at different point locations (model scale): (a) Strongbox1; (b) Strongbox2; (c) Strongbox3; (d) Strongbox4.

### 5. Monotonic Loading

Under monotonic vertical loading, the bucket is penetrated to around 10 mm (0.25L) deeper than the touchdown point to obtain the vertical capacities  $V_0$ ; Figure 8 shows them as hollowed points.  $V_0$  measured at four strongboxes are 129.3, 168.0, 160.6, and 107.8 N, respectively.

To testify the reliability of the centrifuge tests, the vertical capacity is determined using the commercial FE package Plaxis 3D CE V20 [52], in which the bucket is assumed to be wished-in-place, i.e., the bucket is at the touchdown position (Figure 8). The effect caused by installation on the following monotonic loading is considered by reducing the shear stress along the skirt–soil interface. Only half of the bucket and corresponding soil are simulated due to the symmetry of the foundation. To avoid a boundary effect, the soil bottom is  $4L$  away from the bucket tip and the soil sides are  $3.4D$  away from the bucket skirt, as Figure 9 shows. The bucket and soil are discretized with ten-node wedge elements with full integration and the bucket–soil interfaces are composed of twelve-node interface elements. To satisfy the numerical convergence and accuracy, the coarseness factors of mesh are chosen as 1 for the far-field soil, 0.3 for the soil near the bucket ( $0.5D$  horizontally and  $L$  vertically away from the bucket), and 0.1 for the bucket and soil inside the bucket. Clay is regarded as a Tresca material under undrained conditions. The parameters of

undrained shear strength  $s_u$  in each of the monotonic loading tests, including  $s_{um}$  and  $k$ , are deduced from CPTs, as Section 2.2 and Figure 6 describe. Specifically,  $s_u = 6.5 + 0.55z$ ,  $11.6$ ,  $9.0 + 0.4z$ , and  $6.0 + 0.18z$  for Test 1-1 to 4-1, where  $z$  is in the unit of m. The installation effect is considered by reducing the shear stress along the skirt–soil interfaces to  $\alpha s_u$ , where the adhesion factor  $\alpha$  is taken as  $1/S_t$  [8,19]. The value of the adhesion factor is taken as  $\alpha = 0.5$  since the values of  $S_t$  in each strongbox are averaged as 2.1. The typical Young’s modulus of clay is ranged between  $(200 \text{ and } 800)s_u$ , with  $400s_u$  adopted. The effective unit weight of clay is  $6.97 \text{ kN/m}^3$  (see Table 1) and Poisson’s ratio is 0.495 to the approximate constant volume under undrained conditions. The bucket is simplified as a rigid body since the stiffness of the bucket is much higher than that of soil. The center of the bucket top at the mudline level is taken as a reference point, while the load/displacement at the reference point represents that of the whole bucket. The vertical displacement is applied at the reference point, such that the corresponding vertical reaction force of the bucket can be obtained. Similar to that in the tests,  $V_0$  is the reaction force when the vertical displacement reaches  $0.25L$ .

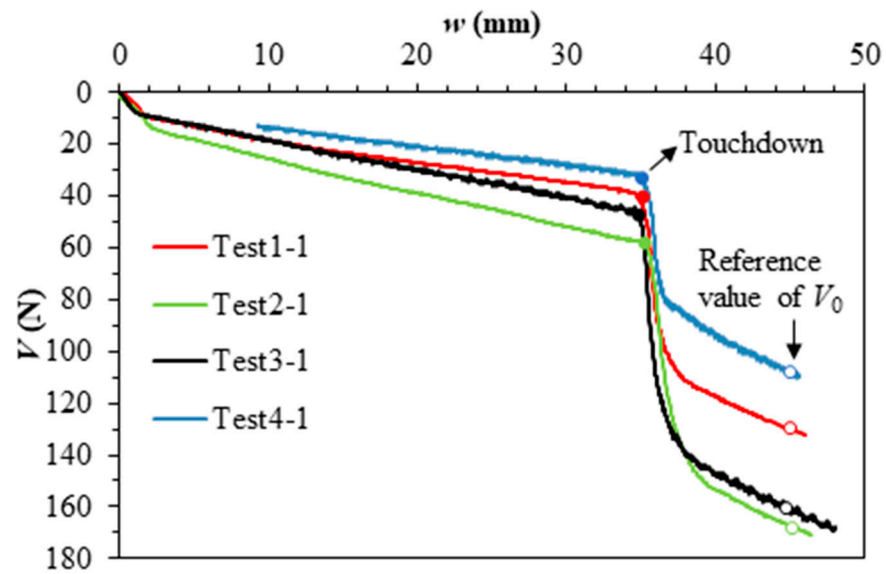


Figure 8. Load–displacement curves under monotonic vertical loading.

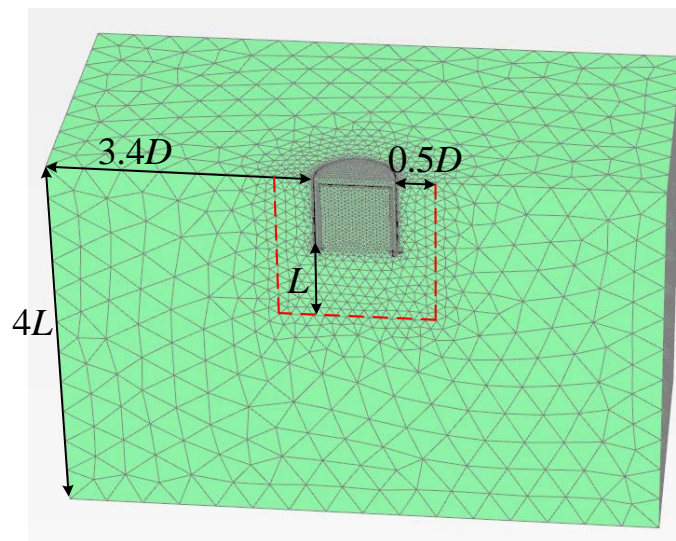


Figure 9. Mesh strategy for the bucket and soil.

Figure 10 presents the monotonic vertical reaction force–displacement curves ( $V - w/L$  curves) by FE. Since the bucket is wished in place in the FE simulation,  $w$  in Figure 10 represents the displacement from the touchdown point. Figure 10 also plots the experimental curves recorded in the tests. The FE values of  $V_0$  at four strongboxes are 132.1, 170.7, 159.8, and 100.8 N, respectively, agreeing well with centrifuge tests with errors less than 6%. The vertical capacity factor of bucket  $N_{cv}$  can be calculated as  $(V_0 - \alpha\pi LDs_{uav})/As_{utip}$ , where  $A$  is the cross-sectional area of the bucket. The corresponding  $N_{cv}$  in four tests are 10.1, 9.5, 10.2, and 10.9, respectively. The errors between  $N_{cv}$  in this study and  $N_{cv} = 10.3$  calculated by the equation proposed by [53] were less than 7%, indicating the reliability of monotonic loading results by centrifuge.

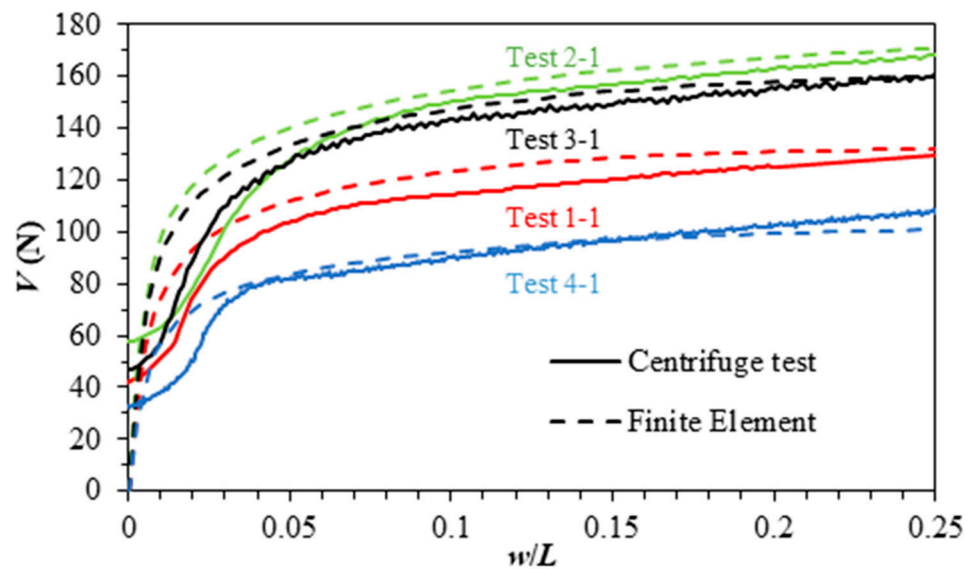


Figure 10. Vertical reaction force–displacement curves ( $V - w/L$  curves) under monotonic loading by FE and centrifuge test.

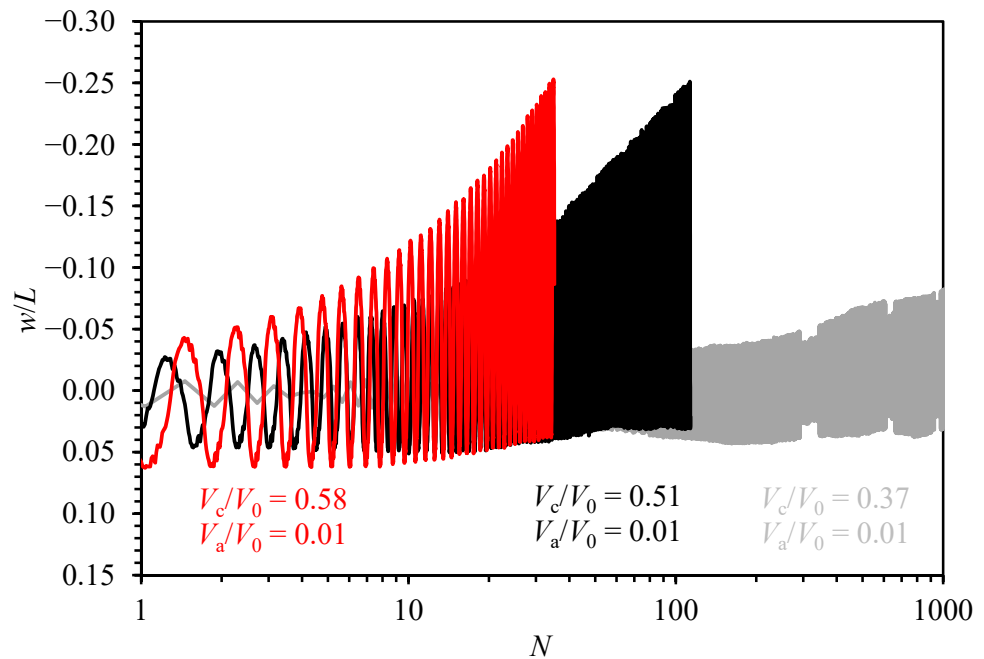
## 6. Cyclic Loading

### 6.1. Evolution of Vertical Displacement

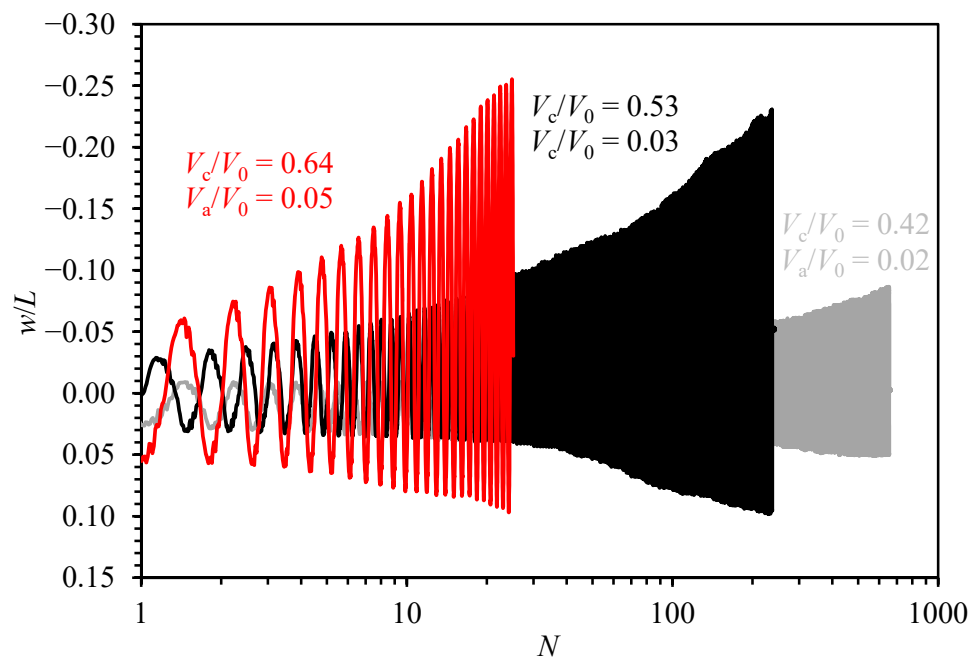
Figure 11 shows the relationships between the normalized vertical displacement  $w/L$  and the number of cycles  $N$ . In Test 3-2 ( $V_c/V_0 = 0.37$ ,  $V_a/V_0 = 0.01$ ), the peak data points near  $N = 300$ , 650, and 900 are not recorded due to signal loss, causing missing parts in the load curves, as Figure 11a shows. The minimum displacements  $w_{min}$  are accumulated upwards under  $V_a/V_0 = 0.01$  in Figure 11a but are accumulated downwards under  $V_a/V_0 = 0.02-0.05$  in Figure 11b. A possible reason is that the evolution of displacements depends on  $V_a/V_0$ , although  $V_a/V_0$  is limited to less than 0.05. The small increase in  $V_a/V_0$  may cause a relatively larger average displacement towards the compression side at the beginning of the tests, affecting the accumulations of average displacements and displacement amplitudes. At the end of the tests, normalized average displacements  $w_a/L$  are between  $-0.024$  and  $-0.109$ . The negative  $w_a$  represents the uplift of the bucket. Similar phenomena were reported by [11].

The negative  $w_a$  under symmetric loading represents that the residual tensile displacements are larger than the compressive ones. The reason is that the tensile capacity of the bucket is lower than the compressive. When cyclic loading into compression is applied, the resistance is composed of the friction along the outside skirt and the end bearing, as Figure 2a shows. The friction along the inside skirt is not mobilized since the soil plug is moved along with the bucket. However, when the cyclic loading into tension is applied, there are three potential failure mechanisms as Figure 2b–d show. In centrifuge tests, the vent of the bucket is sealed after installation, so the negative excess pore pressure is generated inside the bucket, which may prevent the relative movements between the soil

plug and bucket skirt. As a result, the reverse end-bearing mechanism which Figure 2b shows, composed of external friction and reverse end-bearing resistance, occurs.



(a)



(b)

**Figure 11.** Normalized vertical displacement and cyclic number relationship: (a)  $V_c/V_0 = 0.37, 0.51,$  and  $0.58$ ; (b)  $V_c/V_0 = 0.42, 0.53,$  and  $0.64$ .

The external friction of the bucket under compressive and tensile loading are similar to each other, since the soil along the outside of the skirt is roughly under a direct simple shear and the shear stress mobilized is not affected by the loading direction. The contributions of the end-bearing resistance and reverse end-bearing resistance are corresponding to the states of triaxial compression and triaxial tension, respectively. The former is usually larger

due to higher soil strength at the triaxial compression state, i.e., the compressive capacity of the bucket is higher than the tensile. The residual upward displacement of the bucket is thus accumulated gradually even as the symmetrical vertical cyclic loading is applied.

The reverse end-bearing mechanism as Figure 2b shows is proofed further by the soil plug inside the bucket and the shallow pit left on the soil surface after the bucket is pulled out (Figure 12). Under cyclic loading into tension, the soil plug and the soil beneath the bucket tip are mobilized and move upwards along with the bucket due to the negative pressure. Ref. [11] proved the existence of suction by measuring negative excess pore pressure under the bucket lid.



**Figure 12.** Soil plug inside bucket and soil surface after pull-out of bucket: (a) Soil plug inside bucket; (b) Soil surface after pull-out of bucket.

The accumulation rates of  $w_a$  and  $w_c$  are larger under higher  $V_c/V_0$ , as Figure 11 shows. For example, normalized average displacement  $w_a/L$  reaches  $-0.11$  and normalized displacement amplitude  $w_c/L$  reaches  $0.148$  over 35 cycles under  $V_c/V_0 = 0.58$ . As the opposite,  $w_a/L$  is only  $-0.024$  and  $w_c/L$  is  $0.056$  with 996 cycles of  $V_c/V_0 = 0.37$ . The reason may be that the pore pressure is accumulated more under higher  $V_c/V_0$ , causing lower effective stress. So the soil strength is lower under higher  $V_c/V_0$ , leading to larger displacements for the same number of cycles.

Figure 13 shows the hysteresis loop, the relationship between the normalized cyclic loading, and the normalized vertical displacement. To demonstrate the changes of hysteresis loops clearly, Figure 13 demonstrates only the hysteresis loops at typical loading stages, and hysteresis loops without peak data in Test 3-2 ( $V_c/V_0 = 0.37$ ,  $V_a/V_0 = 0.01$ ) are removed. At relatively higher  $V_c/V_0$ , the maximum displacement  $w_{max}$  of the bucket reaches  $0.25L$  over 20–40 cycles, as Figure 13c,f show. At relatively lower  $V_c/V_0$ ,  $w_{max}$  cannot reach  $0.25L$  even under 600–800 cycles, as Figure 13a,d show. Although not measured in this study, the pore pressure may be accumulated much more slowly given that  $V_c/V_0$  is below a threshold, then  $w_{max}$  becomes unchanged with cycles over long-term loading.

For the maximum displacement  $w_{max}$ , the accumulation rate is affected significantly by  $V_c$  and the number of cycles in the tests. At low  $V_c/V_0$  as Figure 13a,d show, the accumulation rate of  $w_{max}$  over 10 cycles is relatively uniform. However, at high  $V_c/V_0$  as Figure 13b,c show, the accumulation rate of  $w_{max}$  over 10 cycles is decreased with  $N$ . The phenomena may be related to the differences in the accumulation rates of pore pressure. At low  $V_c/V_0$ , the pore pressure is accumulated in a relatively uniform rate, while at high  $V_c/V_0$ , the accumulation rate of pore pressure is changed from high to low. Compared to  $w_{max}$ , the accumulation rate of the minimum displacement  $w_{min}$  is always lower. The above phenomena are due to the compressive capacity of the bucket being higher than the tensile one. Compared to the compression, the soil is disturbed more seriously by the tension, and then the strength softening becomes more significant on the tension side.

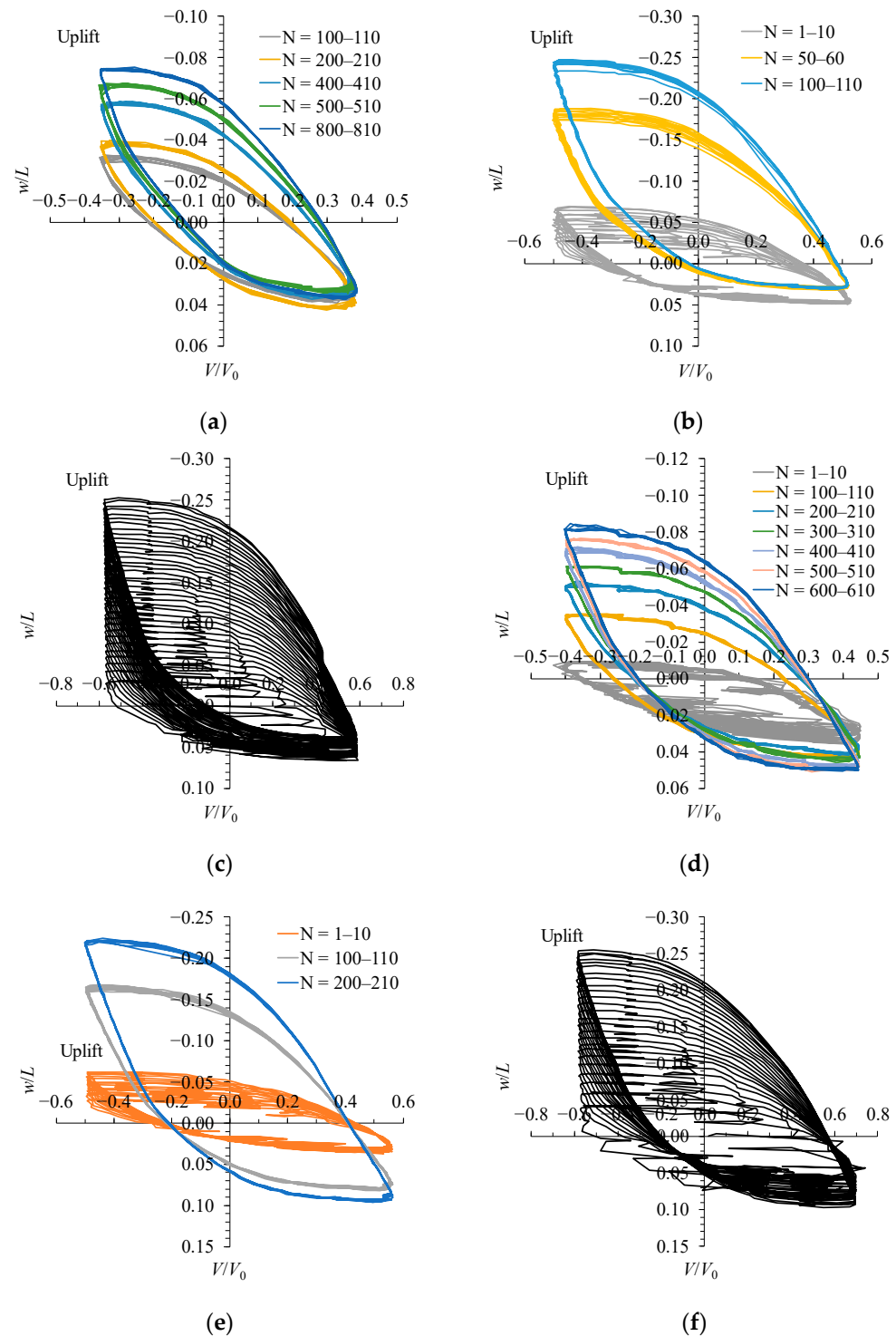


**Figure 13.** Normalized cyclic vertical loading and displacement relationship: (a)  $V_c/V_0 = 0.37$ ,  $V_a/V_0 = 0.01$ ; (b)  $V_c/V_0 = 0.51$ ,  $V_a/V_0 = 0.01$ ; (c)  $V_c/V_0 = 0.58$ ,  $V_a/V_0 = 0.01$ ; (d)  $V_c/V_0 = 0.42$ ,  $V_a/V_0 = 0.02$ ; (e)  $V_c/V_0 = 0.53$ ,  $V_a/V_0 = 0.03$ ; (f)  $V_c/V_0 = 0.64$ ,  $V_a/V_0 = 0.05$ .

### 6.2. Evolution of Secant Stiffness

The secant stiffness  $K_N$  of the  $N$ th hysteresis loop of bucket is defined as the slope of the line connecting the highest and lowest points of the hysteresis loop, as Figure 14 shows. It can be calculated as  $K_N = (V_{\max} - V_{\min}) / (w_{\max} - w_{\min})$  for the  $N$ th cycle.

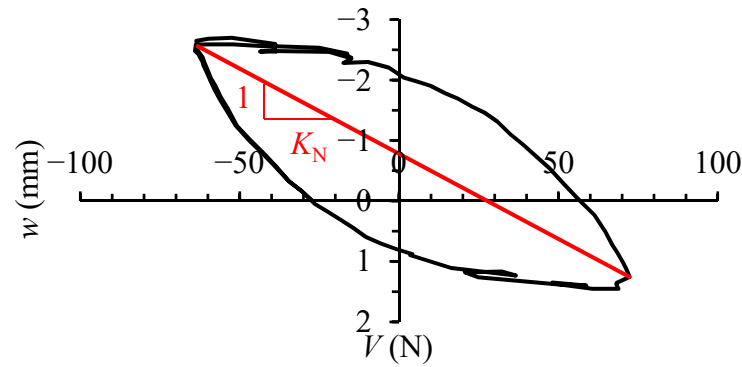


Figure 14. Secant stiffness of hysteresis loop.

Figure 15 shows the relationships between secant stiffness of hysteresis loops and the number of cycles. In general,  $K_N$  is decreased with the increase in  $V_c/V_0$  and  $N$ . The reason may be that high  $V_c/V_0$  or large  $N$  results in the accumulation of excess pore pressures in the soil. At  $V_c/V_0 = 0.51$  and  $0.53$ ,  $K_N$  are close to each other since the loading amplitudes are similar. In Figure 15, the variations of  $K_N$  with  $N$  become gentle at  $V_c/V_0 = 0.37$  and  $0.42$ . It might be due to the fact that the soil around the bucket undergoes partial consolidation after a long-term loading. For example, the loading time is as large as 137 d in the prototype after 996 cycles with  $V_c/V_0 = 0.37$ . Also, the corresponding dimensionless time factor  $T$  after 996 cycles is at least  $0.18$ , exceeding  $T < 1.3 \times 10^{-3}$  for undrained clay as mentioned in Section 3. Therefore, partial drainage may occur in clay and cause an increase in shear strength.

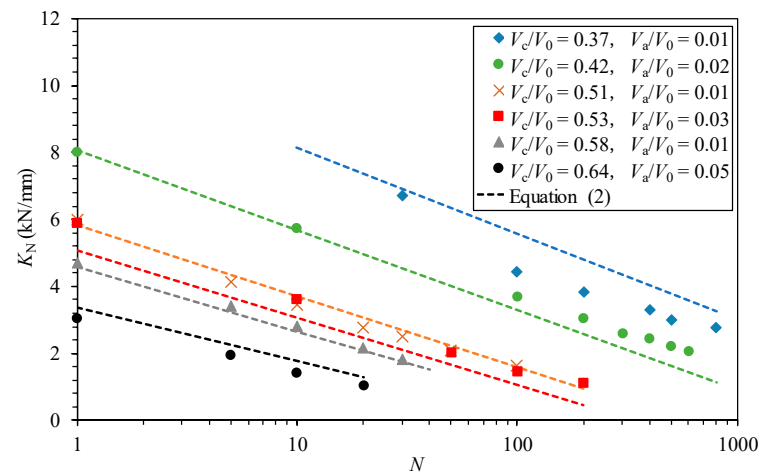


Figure 15. Relationship between secant stiffness of hysteresis loops and cyclic numbers (prototype scale).

By referring to the logarithmic function proposed by [20,54], the relationship between secant stiffness  $K_N$  and the number of cycles  $N$  is expressed as:

$$K_N = K_1 + A_K \ln N, \tag{2}$$

where  $K_1$  is the secant stiffness of the first cycle and  $A_K$  is the fitting parameter.  $K_1$  and  $A_K$  depend on  $\zeta_b (=V_{max}/V_0)$ , as Figure 16a,b show. Figure 15 also demonstrates the predictions of  $K_N$  by Equation (2).

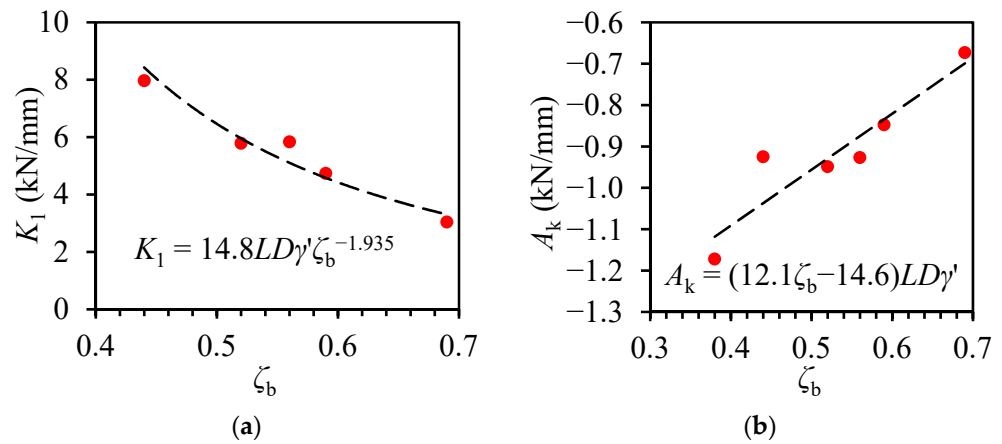


Figure 16. Fitting curves between  $K_1$  and  $A_k$  with  $\zeta_b$  (prototype scale): (a)  $K_1$  with  $\zeta_b$ ; (b)  $A_k$  with  $\zeta_b$ .

To describe the stiffness independent of  $\zeta_b$ , the dimensionless variation in vertical displacement within one cycle  $(w_{max} - w_{min})/L$  and the dimensionless secant stiffness  $K^* = K_N/(V_0/L)$  are adopted by referring to [11]. As Figure 17 shows,  $K^*$  is gradually decreased with the increase in  $(w_{max} - w_{min})/L$  and  $K^*$  is scattered in a relatively narrow range under the different loading amplitude ratio  $V_c/V_0$ . At the same  $(w_{max} - w_{min})/L$ ,  $K^*$  is slightly increased with  $V_c/V_0$ . The evolution of  $K^*$  with  $(w_{max} - w_{min})/L$  can be fitted as:

$$K^* = 1.5[(w_{max} - w_{min})/L]^{-0.8}, \tag{3}$$

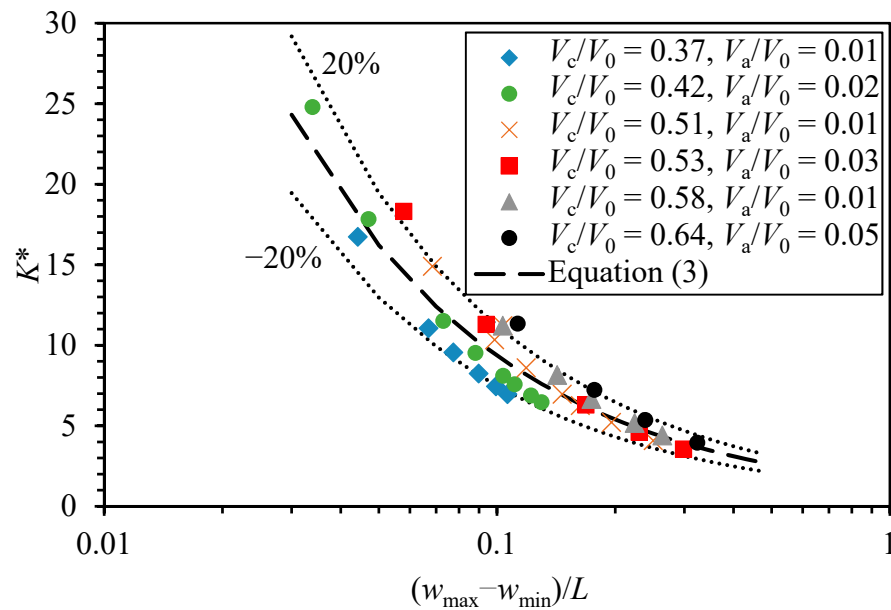


Figure 17. Relationship between dimensionless secant stiffness  $K^*$  and dimensionless variation in vertical displacement within one cycle (the error ranges between results by Equation (3) and tests are shown as dotted lines).

Figure 17 shows the fitting results of Equation (3) as the black dash line. The error between the fitting curve and the test results is within  $\pm 20\%$ .

### 7. Conclusions

The monotonic vertical capacity and cyclic responses of a single bucket under symmetric vertical loading have been studied through centrifuge tests. The loading amplitude

ratio  $V_c/V_0$  is varied between 0.37 and 0.64 to investigate its effects on displacement and stiffness of the bucket. The main conclusions are as follows:

- (1) The vertical capacities by centrifuge tests and numerical simulations are with errors less than 6%. The vertical capacity factors are in the range of 9.5–10.9.
- (2) Under symmetric vertical loading, the normalized average displacements of the bucket, varied between  $-0.024$  and  $-0.109$  in six tests, are on the tensile side due to the tensile capacity being lower than the compressive. The accumulation rates of average displacement and displacement amplitude of the bucket are larger under higher  $V_c/V_0$  due to the lower effective stress.
- (3) The secant stiffness of the bucket is decreased with  $V_c/V_0$  and  $N$ . Partial drainage may occur over 996 cycles with  $V_c/V_0 = 0.37$ , due to the loading time in the prototype of 137 d and the dimensionless time factor  $T > 0.18$ . Based on the experimental results, two simplified equations are proposed to describe the evolution of the secant stiffness of the bucket.

**Author Contributions:** Conceptualization, D.W., J.J. and D.F.; methodology, J.J.; software, D.W. and J.J.; validation, D.W., J.J. and D.F.; formal analysis, J.J.; investigation, D.W., J.J. and D.F.; data curation, J.J.; writing—original draft preparation, J.J.; writing—review and editing, D.W. and D.F.; funding acquisition, D.W. All authors have read and agreed to the published version of the manuscript.

**Funding:** This research was funded by the National Natural Science Foundation of China (grant Nos. 42025702 and 42177122).

**Institutional Review Board Statement:** Not applicable.

**Informed Consent Statement:** Not applicable.

**Data Availability Statement:** Not applicable.

**Conflicts of Interest:** The authors declare no conflict of interest.

## References

1. Housby, G.; Byrne, B. Suction Caisson Foundations for Offshore Wind Turbines and Anemometer Masts. *Wind Eng.* **2000**, *24*, 249–255. [[CrossRef](#)]
2. Faizi, K.; Faramarzi, A.; Dirar, S.; Chapman, D. Investigating the Monotonic Behaviour of Hybrid Tripod Suction Bucket Foundations for Offshore Wind Towers in Sand. *Appl. Ocean Res.* **2019**, *89*, 176–187. [[CrossRef](#)]
3. Randolph, M.; Gourvenec, S. *Offshore Geotechnical Engineering*, 1st ed.; CRC Press: London, UK, 2011; ISBN 978-1-315-27247-4.
4. Vulpe, C. Design Method for the Undrained Capacity of Skirted Circular Foundations under Combined Loading: Effect of Deformable Soil Plug. *Géotechnique* **2015**, *65*, 669–683. [[CrossRef](#)]
5. Achmus, M.; Kuo, Y.S.; Abdel-Rahman, K. Behavior of Monopile Foundations under Cyclic Lateral Load. *Comput. Geotech.* **2009**, *36*, 725–735. [[CrossRef](#)]
6. Jeong, Y.; Kim, J.H.; Park, H.J.; Kim, D. Cyclic Behavior of Unit Bucket for Tripod Foundation System Supporting Offshore Wind Turbine via Model Tests. *Wind Energy* **2018**, *22*, 257–268. [[CrossRef](#)]
7. Housby, G.T.; Kelly, R.B.; Huxtable, J.; Byrne, B.W. Field Trials of Suction Caissons in Clay for Offshore Wind Turbine Foundations. *Géotechnique* **2005**, *55*, 287–296. [[CrossRef](#)]
8. He, B.; Jiang, J.; Cheng, J.; Zheng, J.; Wang, D. The Capacities of Tripod Bucket Foundation under Uniaxial and Combined Loading. *Ocean Eng.* **2021**, *220*, 108400. [[CrossRef](#)]
9. Kim, D.J.; Choo, Y.W.; Kim, J.H.; Kim, S.; Kim, D.S. Investigation of Monotonic and Cyclic Behavior of Tripod Suction Bucket Foundations for Offshore Wind Towers Using Centrifuge Modeling. *J. Geotech. Geoenvironmental Eng.* **2014**, *140*, 04014008. [[CrossRef](#)]
10. Carbon Trust. *Suction Installed Caisson Foundations for Offshore Wind: Design Guidelines*, 1st ed.; Carbon Trust: London, UK, 2019; pp. 1–92.
11. Villalobos, F.A.; Byrne, B.W.; Housby, G.T. Model Testing of Suction Caissons in Clay Subjected to Vertical Loading. *Appl. Ocean Res.* **2010**, *32*, 414–424. [[CrossRef](#)]
12. Jeong, Y.; Ko, K.W.; Kim, D.S.; Kim, J.H. Studies on Cyclic Behavior of Tripod Suction Bucket Foundation System Supporting Offshore Wind Turbine Using Centrifuge Model Test. *Wind Energy* **2020**, *24*, 515–529. [[CrossRef](#)]
13. Wang, Y.; Zhang, S.; Xu, H.; Zhang, Y.; Gaunt, P.; Ren, B.; Zhang, Y.; Yubin, R. Site Investigation and Soil Parameters for Offshore Suction Bucket Design: A Case Study of Houhu Wind Turbine. *Ocean Eng.* **2022**, *255*, 111458. [[CrossRef](#)]
14. Lau, B.H. Cyclic Behaviour of Monopile Foundations for Offshore Wind Turbines in Clay. Ph.D. Thesis, University of Cambridge, Cambridge, UK, 2015.

15. Bransby, M.F.; Yun, G.J. The Undrained Capacity of Skirted Strip Foundations under Combined Loading. *Géotechnique* **2009**, *59*, 115–125. [[CrossRef](#)]
16. Hung, L.C.; Kim, S.R. Evaluation of Vertical and Horizontal Bearing Capacities of Bucket Foundations in Clay. *Ocean Eng.* **2012**, *52*, 75–82. [[CrossRef](#)]
17. Cassidy, M.J.; Byrne, B.W.; Randolph, M.F. A Comparison of the Combined Load Behaviour of Spudcan and Caisson Foundations on Soft Normally Consolidated Clay. *Géotechnique* **2004**, *54*, 91–106. [[CrossRef](#)]
18. Gourvenec, S.; Acosta-Martinez, H.E.; Randolph, M.F. Experimental Study of Uplift Resistance of Shallow Skirted Foundations in Clay under Transient and Sustained Concentric Loading. *Géotechnique* **2009**, *59*, 525–537. [[CrossRef](#)]
19. Supachawarote, C. Inclined Load Capacity of Suction Caisson in Clay. Ph.D. Thesis, University of Western Australia, Perth, Australia, 2006.
20. Leblanc, C.; Houlsby, G.T.; Byrne, B.W. Response of Stiff Piles in Sand to Long-Term Cyclic Lateral Loading. *Géotechnique* **2010**, *60*, 79–90. [[CrossRef](#)]
21. Byrne, B.; Houlsby, G. Experimental Investigations of Response of Suction Caissons to Transient Vertical Loading. *J. Geotech. Geoenvironmental Eng.* **2002**, *128*, 926–939. [[CrossRef](#)]
22. Byrne, B.; Houlsby, G. Experimental Investigations of the Response of Suction Caissons to Transient Combined Loading. *J. Geotech. Geoenvironmental Eng.* **2004**, *130*, 240–253. [[CrossRef](#)]
23. Senders, M. Suction Caissons in Sand as Tripod Foundations for Offshore Wind Turbines. Ph.D. Thesis, University of Western Australia, Perth, Australia, 2009.
24. Bienen, B.; Klinkvort, R.T.; O’Loughlin, C.D.; Zhu, F.; Byrne, B.W. Suction Caissons in Dense Sand, Part II: Vertical Cyclic Loading into Tension. *Géotechnique* **2018**, *68*, 953–967. [[CrossRef](#)]
25. Stapelfeldt, M.; Bienen, B.; Grabe, J. Influence of Low-Permeability Layers on the Installation and the Response to Vertical Cyclic Loading of Suction Caissons. *J. Geotech. Geoenvironmental Eng.* **2021**, *147*, 04021076. [[CrossRef](#)]
26. Kelly, R.; Houlsby, G.; Byrne, B. A Comparison of Field and Laboratory Tests of Caisson Foundations in Sand and Clay. *Géotechnique* **2006**, *56*, 617–626. [[CrossRef](#)]
27. Zhang, Y.; Sudhakaran, K.; Askarinejad, A. Centrifuge Modelling of Suction Caissons Subjected to Cyclic Loading in Tension. In Proceedings of the 4th European Conference on Physical Modelling in Geotechnics, Lulea, Sweden, 15 March 2020.
28. Gütz, P.; Achmus, M. Suction Bucket Foundations under Cyclic Tensile Loading—Physical and Numerical Modeling. *Geotech. Test. J.* **2021**, *44*, 20200056. [[CrossRef](#)]
29. Kou, H.; Fang, W.; Zhou, N.; Huang, J.; Zhang, X. Dynamic Response of Single-Bucket Foundation in Clay under Vertical Variable Amplitude Cyclic Loadings. *Ocean Eng.* **2023**, *273*, 113973. [[CrossRef](#)]
30. Chen, W.; Randolph, M. Uplift Capacity of Suction Caissons under Sustained and Cyclic Loading in Soft Clay. *J. Geotech. Geoenvironmental Eng.* **2007**, *133*, 1352–1363. [[CrossRef](#)]
31. Zografou, D.; Gourvenec, S.; O’Loughlin, C. Vertical Cyclic Loading Response of Shallow Skirted Foundation in Soft Normally Consolidated Clay. *Can. Geotech. J.* **2018**, *56*, 473–483. [[CrossRef](#)]
32. Iskander, M.; El-Gharbawy, S.; Olson, R. Performance of Suction Caissons in Sand and Clay. *Can. Geotech. J.* **2002**, *39*, 576–584. [[CrossRef](#)]
33. Al-Janabi, H.; Aubeny, C. Experimental and Numerical Investigation of the Performance of Piles and Suction Caissons Subjected to Inclined Cyclic Loading in Cohesive Soils. *J. Geotech. Geoenvironmental Eng.* **2022**, *148*, 04022036. [[CrossRef](#)]
34. Wang, T.; Yu, S.; Liu, W.; Bao, X.; Liu, J. Cyclic Bearing Mechanism of Suction Caissons Supporting Offshore Wind Turbines in Clay. *China Ocean Eng.* **2021**, *35*, 135–144. [[CrossRef](#)]
35. Zhou, N.; Kou, H.; Chen, Q. Horizontal Cyclic Response of Bucket Caisson for Offshore Wind Turbines in Over-Consolidated Clay. *Appl. Ocean Res.* **2021**, *118*, 102973. [[CrossRef](#)]
36. Zhao, X.L.; Wang, X.; Ding, P.C.; Sui, S.H.; Deng, W.N. Development and Influence of Pore Pressure around a Bucket Foundation in Silty Soil. *J. Mar. Sci. Eng.* **2022**, *10*, 2020. [[CrossRef](#)]
37. Zhu, W.; Dai, G.; Wang, B.; Gong, W.; Sun, J.; Hu, H. Study on cyclic characteristics and equivalent cyclic creep model of the soft clay at the bottom of suction caisson foundation. *ROCK SOIL Mech.* **2022**, *43*, 466–478. [[CrossRef](#)]
38. Vicent, S.; Kim, S.R.; Van Tung, D.; Bong, T. Effect of Loading Rate on the Pullout Capacity of Offshore Bucket Foundations in Sand. *Ocean Eng.* **2020**, *210*, 107427. [[CrossRef](#)]
39. Chung, S.F.; Randolph, M.F.; Schneider, J.A. Effect of Penetration Rate on Penetrometer Resistance in Clay. *J. Geotech. Geoenvironmental Eng.* **2006**, *132*, 1188–1196. [[CrossRef](#)]
40. Lehane, B.M.; O’loughlin, C.D.; Gaudin, C.; Randolph, M.F. Rate Effects on Penetrometer Resistance in Kaolin. *Géotechnique* **2009**, *59*, 41–52. [[CrossRef](#)]
41. Zhang, W.; Liu, K.; Wang, D.; Zheng, J. Coefficient of Consolidation Measured by Cone Penetration Tests in Overconsolidated Cohesive Soils. *Ocean Eng.* **2023**, *276*, 114301. [[CrossRef](#)]
42. Lunne, T.; Robertson, P.; Powell, J. Cone Penetration Testing in Geotechnical Practice. *Soil Mech. Found. Eng.* **1997**, *46*, 237. [[CrossRef](#)]
43. Low, H.E.; Lunne, T.; Andersen, K.H.; Sjørsen, M.A.; Li, X.; Randolph, M.F. Estimation of Intact and Remoulded Undrained Shear Strengths from Penetration Tests in Soft Clays. *Géotechnique* **2010**, *60*, 843–859. [[CrossRef](#)]

44. Liu, B.; Zhang, Y.; Ma, Z.; Andersen, K.; Jostad, H.; Liu, D.; Pei, A. Design Considerations of Suction Caisson Foundations for Offshore Wind Turbines in Southern China. *Appl. Ocean Res.* **2020**, *104*, 102358. [[CrossRef](#)]
45. Dong, Y.K.; Wang, D.; Randolph, M. Investigation of Impact Forces on Pipeline by Submarine Landslide with Material Point Method. *Ocean Eng.* **2017**, *146*, 21–28. [[CrossRef](#)]
46. Sun, Q.L.; Wang, Q.; Shi, F.Y.; Alves, T.; Gao, S.; Xie, X.N.; Wu, S.G.; Li, J.B. Runup of Landslide-generated Tsunamis Controlled by Paleogeography and Sea-level Change. *Commun. Earth Environ.* **2022**, *3*, 244. [[CrossRef](#)]
47. Randolph, M.F. Offshore Design Approaches and Model Tests for Sub-Failure Cyclic Loading of Foundations. In *Mechanical Behaviour of Soils under Environmentally Induced Cyclic Loads*; Di Prisco, C., Wood, D.M., Eds.; CISM Courses and Lectures; Springer: Vienna, Austria, 2012; pp. 441–480. ISBN 978-3-7091-1068-3.
48. Zhu, F.Y.; O’Loughlin, C.D.; Bienen, B.; Cassidy, M.J.; Morgan, N. The Response of Suction Caissons to Long-Term Lateral Cyclic Loading in Single-Layer and Layered Seabeds. *Géotechnique* **2018**, *68*, 729–741. [[CrossRef](#)]
49. Gourvenec, S.; Randolph, M. Consolidation beneath Circular Skirted Foundations. *Int. J. Geomech.* **2010**, *10*, 22–29. [[CrossRef](#)]
50. Feng, X.; Gourvenec, S. Consolidated Undrained Load-Carrying Capacity of Subsea Mudmats under Combined Loading in Six Degrees of Freedom. *Géotechnique* **2015**, *65*, 563–575. [[CrossRef](#)]
51. DNV-RP-E303 Geotechnical Design and Installation of Suction Anchors in Clay. Available online: <https://www.dnv.com/Default> (accessed on 22 October 2023).
52. Manuals-PLAXIS-GeoStudio | PLAXIS Wiki-GeoStudio | PLAXIS-Bentley Communities. Available online: <https://communities.bentley.com/products/geotech-analysis/w/wiki/46137/manuals-{}-{}-plaxis> (accessed on 25 September 2023).
53. Kanmin, S.; Jiang, J.; Wang, D.; Zheng, J. Capacities of Tripod Bucket Foundation under Uniaxial and Combined Loading Considering Adhesion Factor. *Mar. Georesources Geotechnol.* **2021**, *40*, 1520–1528. [[CrossRef](#)]
54. Hung, L.C.; Lee, S.H.; Vicent, S.; Kim, S.R. An Experimental Investigation of the Cyclic Response of Bucket Foundations in Soft Clay under One-Way Cyclic Horizontal Loads. *Appl. Ocean Res.* **2018**, *71*, 59–68. [[CrossRef](#)]

**Disclaimer/Publisher’s Note:** The statements, opinions and data contained in all publications are solely those of the individual author(s) and contributor(s) and not of MDPI and/or the editor(s). MDPI and/or the editor(s) disclaim responsibility for any injury to people or property resulting from any ideas, methods, instructions or products referred to in the content.